Electronic Supplemental Information for:

Polyoxometalate-encapsulated nanocage cluster organic framework built by {Cu$_4$P$_2$} units and its efficient bifunctional electrochemical performance†

Shaobin Li,*,† Xiaoguo Tan,† Ming Yue,§ Li Zhang,*,† Dongfeng Chai,‡ Wendi Wang,† Hong Pan,† Linlin Fan,† and Chunyan Zhao‡

†College of Materials Science and Engineering, Qiqihar University, Key Laboratory of Polymeric Composite Materials of Heilongjiang Province, Qiqihar 161006, P. R. China.

‡College of Chemistry and Chemical Engineering, Qiqihar University, Qiqihar 161006, P. R. China.

§School of Materials Science and Engineering, East China University of Science and Technology, Shanghai 200237, P. R. China

Table of Contents

Section 1 Experimental Section

Section 2 Supplementary Structural Information

Section 3 Supplementary Physical Characterizations

Section 1 Experimental Section

I. Materials and General Methods

All reagents were purchased commercially and were used without further purification. Elemental analyses (C, H and N) were performed on a Perkin-Elmer 2400 CHN Elemental Analyzer, and that of Cu, Mo were carried out with a Leaman inductively coupled plasma (ICP) spectrometer. The FT-IR spectra were recorded from KBr pellets in the range of 4000–400 cm^{-1} with a Nicolet AVATAR FT-IR360 spectrometer. The powder X-ray diffraction (PXRD) data were collected on a Rigaku RINT 2000 diffractometer at room temperature. The N_2 absorption measurement was performed on autosorb-iQ$_2$ apparatuses at 77 K. X-ray photoelectron spectroscopy (XPS) analyses were performed on an ESCALAB-MKII spectrometer with Mg Kα X-ray radiation as the X-ray source for excitation. All the electrochemical measurements were carried out on Metrohm PGSTAT 128N electrochemical workstation. A conventional three-electrode system was used, with a glassy carbon electrode (GCE) as a working electrode, a commercial Ag/AgCl as reference electrode and platinum wire as counter electrode. Electrochemical Impedance Spectroscopy (EIS) measurement was measured in the frequency range 0.005 Hz to 100 kHz. The specific gravimetric capacitance value can be calculated from the following equation:

$$C_s = \frac{I\Delta t}{m\Delta V}$$

where Cs (F g^{-1}) represents the specific capacitance, I (A) represents the discharge current, ΔV (V) represents the potential change within the discharge time Δt (s), and m (g) corresponds to the amount of active material on the electrode.[1]

II. Synthesis of compound 1

A mixture of $H_3PMo_{12}O_{40}$ (0.22 g, 0.12 mmol), $CuCl_2\cdot6H_2O$ (0.15 g, 0.6 mmol), $C_6H_5PO_3$ (0.04 g, 0.25 mmol) and bimb (0.08 g, 0.38 mmol) were dissolved in 10 mL of MeOH/H_2O (2:3) at room temperature. After the pH value of the mixture was adjusted to about 3.8, the suspension was put into a Teflon-lined autoclave and kept

under autogenous pressure at 120 °C for 56 hours. After slow cooling to room temperature, blackish green polyhedral crystals of **1** were filtered, washed with distilled water and dried at room temperature (Fig.S1). Yield: 52 % (based on Mo). The reproducibility of **1** is good. Elemental analysis calc (%) for $C_{60}H_{57}Cu_4Mo_{12}N_{16}O_{50}P_3$: C 21.83, H 1.74, N 6.79, Cu 7.70, Mo 34.88 %; Found: C 21.79, H 1.77, N 6.83, Cu 7.75, Mo 34.96 %.

III. X-ray Crystallography

Single-crystal X-ray diffraction data collection of compound **1** was performed using a Bruker Smart Apex CCD diffractometer with Cu-*Ka* radiation ($\lambda = 0.71073$ Å) at 293 K. Absorption correction was applied by using the multi-scan program SADABS.[2] The structure was solved by the direct method, and non-hydrogen atoms were refined anisotropically by least-squares on F^2 using the SHELXTL program.[3] The hydrogen atoms of organic ligands were generated geometrically for **1**, while the hydrogen atoms of water molecules can not be found from the residual peaks and were directly included in the final molecular formula. Crystallographic data for the structures reported in this paper have been deposited in the Cambridge Crystallographic Data Center with CCDC Number: 2034009.

Table S1. Crystal data and structure refinements for **1**.

Compound	1
Formula	$C_{60}H_{57}Cu_4Mo_{12}N_{16}O_{50}P_3$
Formula weight	3300.55
Crystal system	Monoclinic
Space group	*C2/m*
a/Å	24.841(6)

b/Å	18.316(4)
c/Å	10.897(5)
β/°	105.586(4)
V/Å^3	4776(3)
Z	2
D_{calcd}/g cm^{-3}	2.290
T/K	293(2)
μ/mm^{-1}	2.538
Refl. Measured	13369
Refl. Unique	4365
R_{int}	0.0821
GoF on F^2	0.769
R_1/wR_2 [$I{\geq}2\sigma(I)$]	0.0617/0.2170

$$R_I = \sum \left| \left| F_o \right| - \left| F_c \right| \right| / \sum \left| F_o \right| . \; wR_2 = \sum[w(F_o{}^2 - F_c{}^2)^2]/\sum[w(F_o{}^2)^2]^{1/2}$$
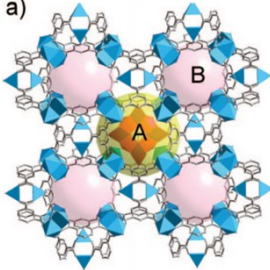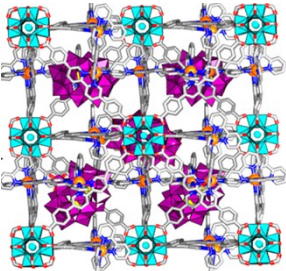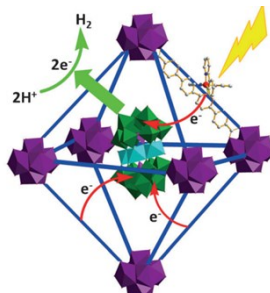
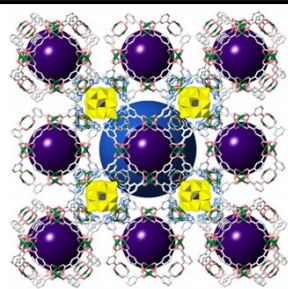## IV. Preparation of the Modified Electrodes

Prior to be modified, the glassy carbon (GCE) working electrode was polished carefully before each experiment with 0.05 μm alumina powders on chamois leather and then cleaned with HNO_3 (1:1), ethanol, and deionized water, respectively.

To prepare the working electrode of **1**-based and **PMo$_{12}$**-based electrodes, a mixture of the desired amount of as-synthesized samples (20 mg) and acetylene black in a weight ratio of 1:1 was co-grounded in a mortar for 45 min. Catalyst ink was prepared by mixing 16 mg of the prepared catalyst powders into 0.25 mL of ethyl alcohol and 0.75 mL of deionized water, and then ultrasonically dispersed for 45 min. Then 5 μL of well dispersed slurry was transferred onto the clean-washed GCE and dried for at least 5 hours in air at room temperature in order to form a uniform thin film.

Section 2 Supplementary Structural Section

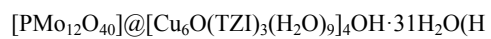**Table S2.** Summary of the known POM@ cluster organic frameworks.

No.	Compounds	Metal clusters	POM types	References
1	 $[Cu_2(BTC)_{4/3}(H_2O)_2]_6[H_nXM_{12}O_{40}]\cdot(C_4H_{12}N)_2$ (X = Si, Ge, P, As; M = W, Mo)	Cu2-Cluster	Keggin	*Liu group,* **J. Am. Chem. Soc.** 2009, 131, 1883.[4]
2	 $(P_2W_8O_{62})@[Zr_6(\mu_3\text{-}O)_4(\mu_3\text{-}OH)_4(L)_6](CO_2CF_3)_{12}$	Zr6-Cluster	Dawson	*Lin group,* **J. Am. Chem. Soc.** 2015, 137, 3197.[5]
3	 $[Ni_4(H_2O)_2(PW_9O_{34})_2]@[Zr_6(\mu_3\text{-}O)_4(\mu_3\text{-}OH)_4(L)_6](CO_2CF_3)_6$	Zr6-Cluster	$Ni_4(H_2O)_2(PW_9O_{34})_2$	*Lin group,* **Angew. Chem. Int . Ed.** 2016, 55, 1.[6]
4				

	Cu2/Cu3-Clusters	Keggin	*Yan group., Sci Rep.*, 2016, 6, 25595.[7]

[PMo$_{12}$O$_{40}$]@[Cu$_6$O(TZI)$_3$(H$_2$O)$_9$]$_4$OH·31H$_2$O(H

LJU-

1),[SiMo$_{12}$O$_{40}$]@[Cu$_6$O(TZI)$_3$(H$_2$O)$_9$]$_4$·32H$_2$O(H

LJU-

2)[PW$_{12}$O$_{40}$]@[Cu$_6$O(TZI)$_3$(H$_2$O)$_6$]$_4$·OH·31H$_2$O(

HLJU-3)
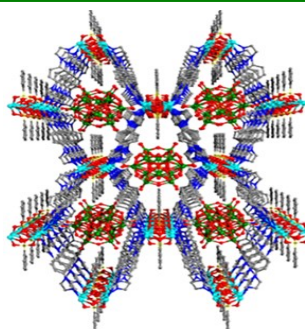
5		Cu4-Cluster	Keggin	This work

[HPMo$_{12}$O$_{40}$]@[Cu$_4$(μ$_2$-OH)$_2$(C$_6$H$_5$PO$_3$)$_2$(bimb)$_4$]
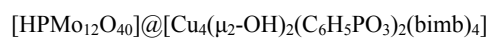
(**1**)
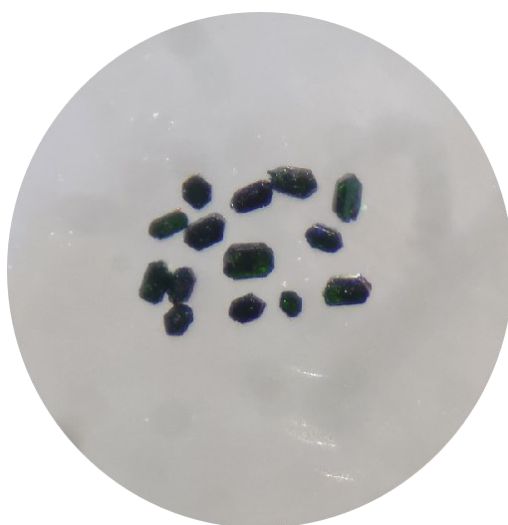

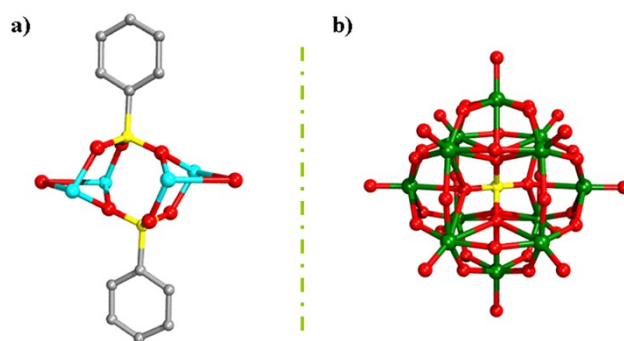**Fig.S1** The images of compound **1** under an optical microscope**.**

Fig.S2 (a) Ball and stick representation of the coordination environments of the Cu_4P_2 cluster SBU-I, and (b) PMo_{12} cluster SBU-II in **1** .
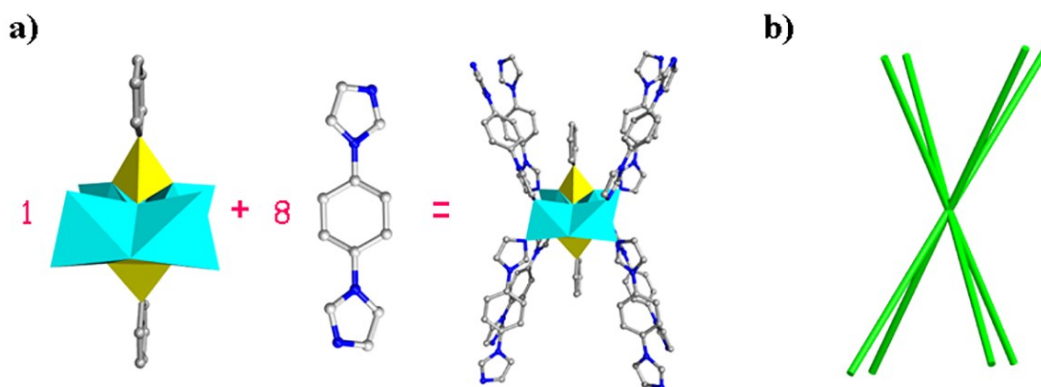

Fig.S3 (a) Cu_4P_2 cluster connected to eight bimb ligands,(b) simplify eight-connected node in **1**.

Section 3 Supplementary Physical Characterizations

I. Analyses of BVS, XPS, IR, PXRD and BET measurements

BVS and XPS: Compound **1** was synthesized under solvothermal conditions. All copper atoms in **1** are in the +II oxidation state, confirmed by their octahedral coordination environments, blue crystal color and BVS calculations.[8] X-ray photoelectron spectroscopy (XPS) is studied for compounds **1** to further confirm the oxidation states of Mo atoms. The XPS survey spectrum confirms that compound **1** contains P, Mo, C, N, O and Cu in Fig. S4a, and the high-resolution XPS spectrum of Mo in compound **1** at about 232.4 and 235.5 eV which are assigned to the $Mo^{VI}3d_{5/2}$ and $Mo^{VI}3d_{3/2}$, respectively (Fig. S4b)[9], and the high-resolution XPS spectrum of Cu in compound **1** at about 934.7.4 and 954.3 eV which are assigned to the $Cu^{II}2P_{1/2}$ and $Cu^{II}2P_{3/2}$, respectively (Fig. S4c)[10]. In addition, for charge balance, since **1** was isolated from acidic aqueous solution, one proton is added to PMo_{12} cluster in the formula of **1**, which is also observed in other compounds such as $[Cu_2(pzta)_2(bipy)_2(H_2O)_2][HPW_{12}O_{40}]$,[11] $[Cu_4(H_2O)(bte)(HPMo_{10}^{VI}Mo_2^{V}O)]\cdot 2H_2O$,[12] and $(Hcpy)[H_2PMo_{12}O_{40}]$.[13]
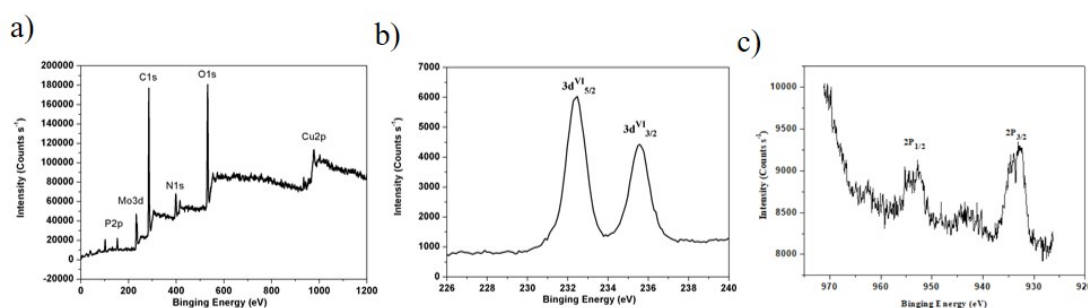

Fig. S4 (a) The XPS survey spectrum of **1**, (b) high-resolution XPS spectrum of Mo (3d) and (c) high-resolution XPS spectrum of Cu (2p).

IR: The IR spectrum exhibits the characteristic peaks at 1063, 968, 897 and 783 cm^{-1} in **1** (Fig. S5), which are attributed to v(P-O), v(Mo=Ot), v_{as}(Mo–Ob–Mo) and v_{as}(Mo–Oc–Mo), respectively.[14] Compared to the typical Keggin type PMo$_{12}$ polyanion, compound **1** has similar peaks in the range of 750–1070 cm^{-1} except for slight shifts of peaks due to the interactions between the polyanions and the Cu(II) ions in the solid state, which indicates that the PMo$_{12}$ cluster in the title compound still retains the basic structure of Keggin PMo$_{12}$ polyanion. Additionally, the characteristic peaks in the region 1628 to 1259 cm^{-1} could be ascribed to the characteristic peaks of bimb ligands.[15]
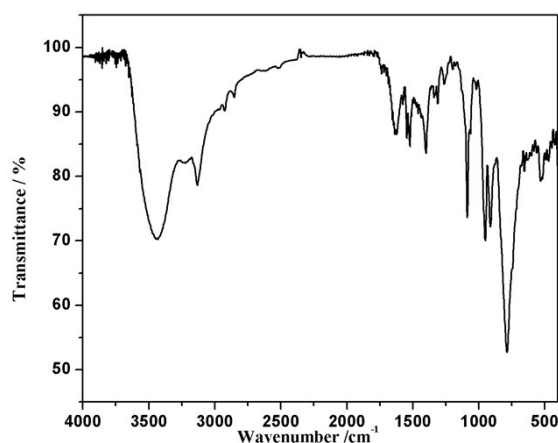

Fig. S5 The IR spectrum of compound **1**.

PXRD: To indicate the phase purity of compound **1**, the PXRD experiment was provided in Fig. S6. The diffraction peaks of both simulated and experimental patterns match well in the key positions, which indicate the phase purity of the title compound is good. The difference in reflection intensities between the simulated and the experimental patterns is due to the different orientation of the crystals in the powder samples.
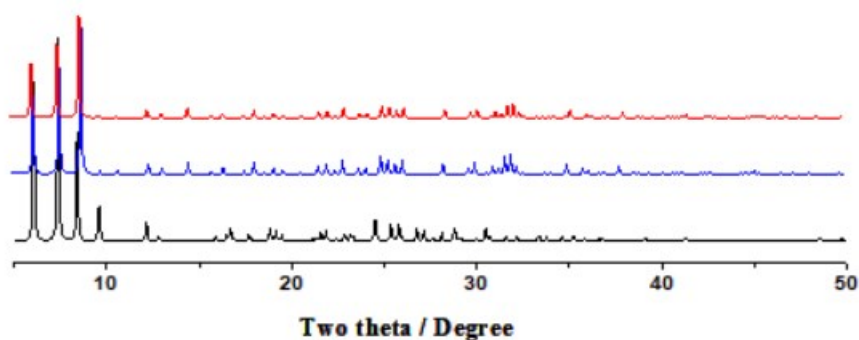
Fig. S6 The simulative (black), experimental (blue) and immersed in 1M H_2SO_4 (about 36 h) (red) of powder X-ray diffraction patterns for **1**.

BET: The BET measurement of **1** has been investigated. Before measurement **1** was degassed at 473 K for 12 h under vacuum. The N_2 adsorption-desorption isotherm of **1** shows a typical type IV isotherm with a hysteresis loop (Fig. S7). The BET surface area was estimated to be 120.1 m^2g^{-1}. Meanwhile, the porosities of **1** are calculated by a *PLATON* programs.[16] Calculations using *PLATON* reveal that the effective free volume is 348.8 $Å^3$ equal to 7.3 % of the crystal volume 4776 $Å^3$ for **1**. The octahedral-like four-nuclear organophosphorus-copper cluster organic framework encapsulated by protonated PMo_{12} providing excellent electronic conductivity, which possess proper BET surface and could facilitate well efficient enhance its electrocatalytic activity.
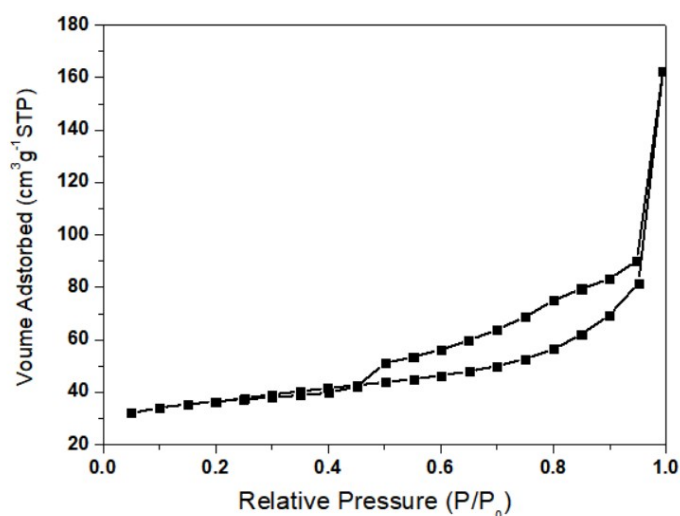

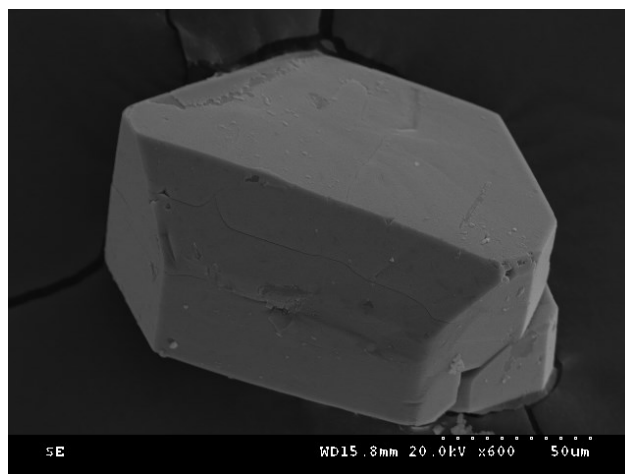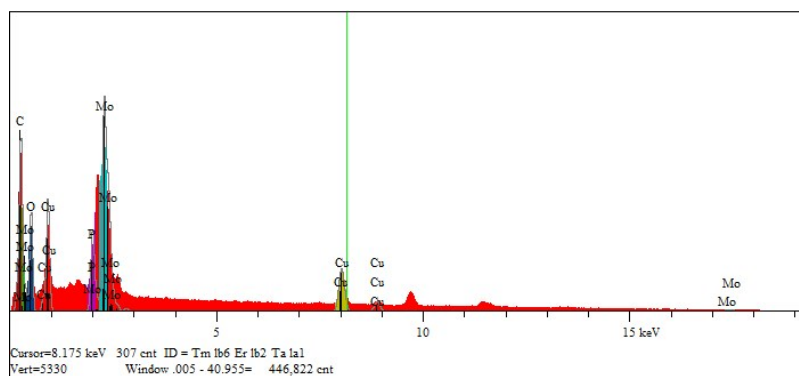**Fig. S7** N_2 adsorption-desorption isotherm curve of **1**.

Fig. S8 The SEM image of **1**.

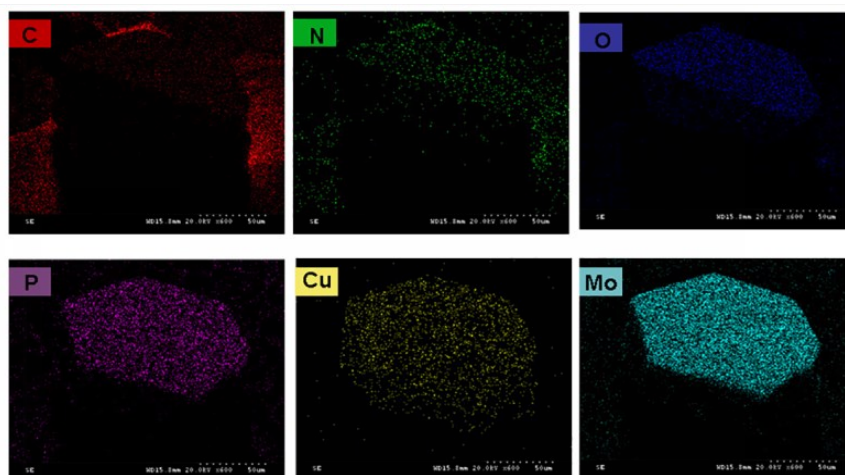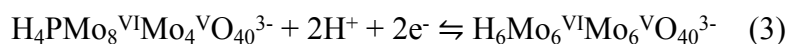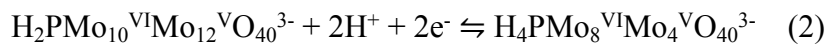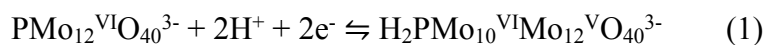**Fig. S9** The EDS analysis of **1**.

Fig. S10 The EDS elemental mapping images of **1**.

II. Equations of electrocatalytic mechanisms

The mechanism of electrocatalytic reaction toward NO_2^- can be described by the

following equations (1-4).

Electrochemical reactions:

$PMo_{12}^{VI}O_{40}^{3-} + 2H^+ + 2e^- \leftrightharpoons H_2PMo_{10}^{VI}Mo_{12}^{V}O_{40}^{3-}$ (1)

$H_2PMo_{10}^{VI}Mo_{12}^{V}O_{40}^{3-} + 2H^+ + 2e^- \leftrightharpoons H_4PMo_8^{VI}Mo_4^{V}O_{40}^{3-}$ (2)

$H_4PMo_8^{VI}Mo_4^{V}O_{40}^{3-} + 2H^+ + 2e^- \leftrightharpoons H_6Mo_6^{VI}Mo_6^{V}O_{40}^{3-}$ (3)

Catalytic chemical steps:

$H_6Mo_6^{VI}Mo_6^{V}O_{40}^{3-} + 6NO_2^- + 6H^+ \rightarrow PMo_{12}^{VI}O_{40}^{3-} + 6NO + 6H_2O$ (4)
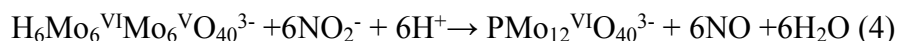
III. Additional figure and table for electrocatalytic experiments
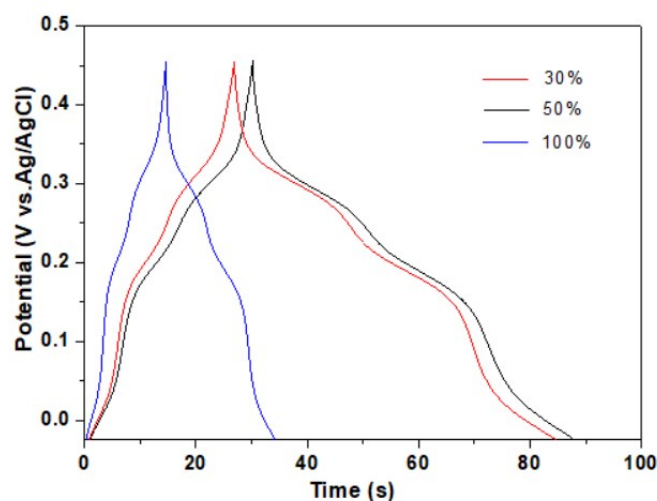
Fig. S11. The GCD curves of different amount of **1**-based electrode at current density of 3 A g^{-1} in 1 M H$_2$SO$_4$ solution (Amount of **1** deposited are 30%, 50%, 100%, respectively).

The Rs is the total ohmic resistance of the solution, CPE1 and CPE2 are the constant phase element, Rd is the diffusion resistance and Rct is the charge-transfer resistance of the electrodes, and W$_o$ is the generalized finite Warburg impedance (Zw) of the solidphase diffusion.

Fig. S12. The equivalent circuit of **1**.

Table S3. Summary of the crystalline POM-based supercapacitor electrode

materials at 5 A g^{-1}.

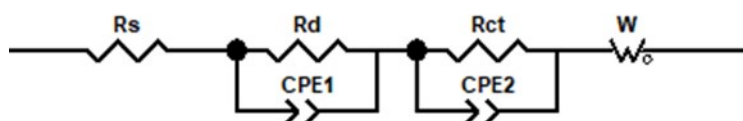| Crystalline POM-based supercapacitor electrode materials	Specific capacitance (F g^{-1})	Ref.
[H(C$_{10}$H$_{10}$N$_2$)Cu$_2$][PMo$_{12}$O$_{40}$]	232	17
[H(C$_{10}$H$_{10}$N$_2$)Cu$_2$][PW$_{12}$O$_{40}$]	106.4	17
(C$_{12}$H$_6$N$_2$)$_3${[Cu(C$_5$H$_3$N$_6$)(H$_2$O)][P$_2$W$_{18}$O$_{62}$]}·5H$_2$O	168	18
[Ag$_5$(C$_9$H$_7$N$_3$Br)$_4$][VW$_{10}$V$_2$O$_{40}$]	206 (110 A g^{-1})	19
[Cu$^I_4$H$_2$(C$_{12}$H$_{12}$N$_6$)$_5$(PW$_{12}$O$_{40}$)$_2$]·2H$_2$O	76.4	20
[Cu^{II}Cu$^I_3$(H$_2$O)$_2$(C$_{12}$H$_{12}$N$_6$)$_5$(PW$^{VI}_{10}$W$^V_2$O$_{40}$)]·2H$_2$O	71.4	20
[Cu$^I_6$(C$_{12}$H$_{12}$N$_6$)$_6$(PW$^{VI}_9$W$^V_3$O$_{40}$)]·2H$_2$O	62.9	20
[Cu$^I_4$H$_2$(C$_{12}$H$_{12}$N$_6$)$_5$(PMo$_{12}$O$_{40}$)$_2$]·2H$_2$O	220.6	20
[Cu^{II}Cu$^I_3$(C$_{12}$H$_{12}$N$_6$)$_5$(SiMo$^{VI}_{11}$Mo^{V}O$_{40}$)]·4H$_2$O	135.7	20
[Cu^{II}(C$_{12}$H$_{12}$N$_6$)$_2$]$_2$[SiW$_{12}$O$_{40}$]	73.1	21
[Cu^I(C$_{12}$H$_{12}$N$_6$)]$_4$[SiW$_{12}$O$_{40}$]	90.4	21
[Cu$^I_4$(C$_{12}$H$_{12}$N$_6$)$_3$][SiW$_{12}$O$_{40}$]·2H$_2$O	45.4	21
[{Cu$^{II}_6$(C$_{12}$H$_{12}$N$_6$)$_7$(H$_2$O)$_{12}$}H$_4$⊂(W$_{12}$O$_{40}$)$_2$]·12H$_2$O	42.3	21
[{Cu$^{II}_7$(C$_{12}$H$_{12}$N$_6$)$_8$(H$_2$O)$_{10}$}H$_2$⊂(W$_{12}$O$_{40}$)$_2$]·2H$_2$O	15.7	21
[{Cu$^{II}_{10}$Cu$^I_2$(C$_{12}$H$_{12}$N$_6$)$_{11}$(H$_2$O)$_{16}$}H$_2$⊂(W$_{12}$O$_{40}$)$_3$]·6H$_2$O	26.4	21
[Ag$_5$(C$_2$H$_2$N$_3$)$_6$][H$_5$⊂SiMo$_{12}$O$_{40}$]@15%GO	230.5 (0.5 A g^{-1})	22
[{Ag$_5$(C$_4$H$_4$N$_2$)$_7$}(BW$_{12}$O$_{40}$)]	1058 (2.16 A g^{-1})	23
[{Ag$_5$(C$_4$H$_4$N$_2$)$_7$}(SiW$_{12}$O$_{40}$)](OH)·H$_2$O	986 (2.16 A g^{-1})	23
(C$_4$H$_6$N)[{Ag(pz)}$_2$(PMo$_{12}$O$_{40}$)]	1611 (2.16 A g^{-1})	23
[Cu$^{II}_2$(C$_{12}$H$_{12}$N$_6$)$_4$(PMo$^{VI}_9$Mo$^V_3$O$_{39}$)]	146.7	24
[Cu^{I}H$_2$(C$_{12}$H$_{12}$N$_6$)(PMo$_{12}$O$_{40}$)]·(C$_6$H$_{15}$N)[(H$_2$O)$_2$]	239.2	24
[HPMo$_{12}$O$_{40}$]@[Cu$_4$(μ$_2$-OH)$_2$(C$_6$H$_5$PO$_3$)$_2$(bimb)$_4$]	267.0	This work
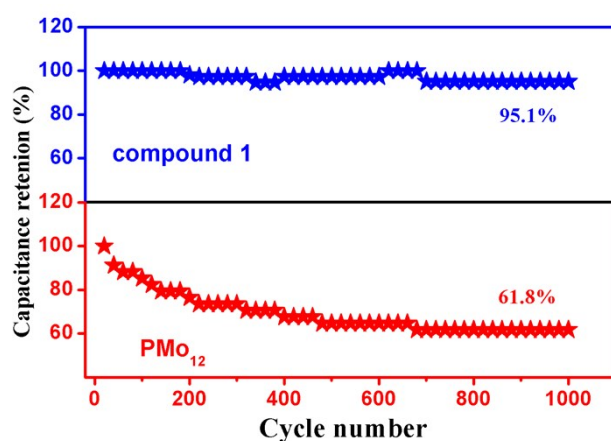
Fig. S13 Cycling stability performances of **1**-(blue) and PMo$_{12}$-(red) based electrodes during 1000 cycle charge/discharge at the current density of 10.0 A g^{-1}.

Reference

1. H. N. Wang, M. Zhang, A. M. Zhang, F. C. Shen, X. K. Wang, S. N. Sun, Y. J. Chen,   Y. Q. Lan, *Acs Appl Mater Inter.,* **2018***,* 10*,* 32265-32270.

2. G. M. Sheldrick, *SADABS 2.05*; University of Göttingen: Göttingen, Germany.

3. *SHELXTL 6.10*; Bruker Analytical Instrumentation: Madison, WI, 2000.

4. C. Y. Sun, S. X. Liu, D. D. Liang, K. Z. Shao, Y. H. Ren, Z. M. Su, *J. Am. Chem. Soc*., 2009, **131**, 1883.

5. Z. M. Zhang, T. Zhang, C. Wang, Z. K. Lin, L. S. Long, W. B. Lin, *J. Am. Chem. Soc*., 2015, **137**, 3197.

6. X. J. Kong, Z. K. Lin, Z. M. Zhang, T. Zhang, W. B. Lin, *Angew. Chem. Int. Ed*., 2016, **55**, 1.

7. J. W. Sun, P. F. Yan, G. H. An, J. Q. Sha, G. M. Li, G. Y. Yang, *Sci Rep*., 2016, **6**, 25595.

8. I. D. Brown and D. Altermatt, *Acta Crystallogr. Sect. B: Struct. Sci.*, 1985, **41**, 244.

9. Y. Dong, L. Chen, W. Chen, X. Zheng, X. Wang, E. Wang, *Chem. Asian J*., 2018, **13**, 3304-3313.

10. D. C. Zhao, Y. Y. Hu, H. Ding, H. Y. Guo, X. B. Cui, X. Zhang, Q. S. Huo, J. Q. Xu, *Dalton Trans*., 2015, **44**, 8971.

11. Y. Y. An, L. Wang, Y. Hu, T. Q. Xu, Y. J. Hou, *Inorg. Chem*., 2016, 55, 144–153.

12. A.X. Tian, J. Ying, J. Peng, J.Q. Sha, H.J. Pang, Y. Chen, Z.M. Su, *Crystal Growth Des*., 2008, 8, 3717–3724.

13. Z.G. Han, Y. Z. Gao, X. L. Zhai, J. Peng, Y. L. Zhao, C. W. Hu, *Crystal Growth Des*., 2009, 9, 1225–1234.

14.X. L. Wang, Y. F. Bi, B. K. Chen, H. Y. Lin, G. C. Liu, *Inorg. Chem*., 2008, **47**,

2442.

15. H. Y. Zang, Y. Q. Lan, S. L. Li, G. S. Yang, K. Z. Shao, X. L. Wang, L. K. Yan and Z. M. Su, *Dalton Trans.*, 2011, **40**, 3176.

16. A. L. Spek, *J. Appl. Crystallogr.*, 2003, **36**, 7.

17. S. Roy, V. Vemuri, S. Maiti, K. S. Manoj, U. Subbarao and S. C. Peter, *Inorg. Chem.*, 2018, **57**, 12078-12092.

18. G. Wang, T. Chen, S. Li, H. Pang and H. Ma, *Dalton Trans.*, 2017, **46**, 13897-13902.

19. G. Wang, T. Chen, X. Wang, H. Ma and H. Pang, *Eur. J. Inorg. Chem.*, 2017, **2017**, 5350-5355.

20. D. F. Chai, C. J. Gómez-García, B. N. Li, H. J Pang, H. Y. Ma, X. M. Wang and L. C. Tan, *Chem. Eng. J.*, 2019, **373**, 587-597.

21. D. Chai, Y. Hou, K. P. O'Halloran, H. Pang, H. Ma, G. Wang and X. Wang, *ChemElectroChem*, 2018, **5**, 3443-3450.

22. Y. Hou, D. F. Chai, B. N. Li, H. J. Pang, H.Y. Ma, X. M. Wang and L. C. Tan, *ACS Appl. Mater. Interfaces*, 2019, **11**, 20845-20853.

23. N. Du, L. Gong, L. Fan, K. Yu, H. Luo, S. Pang, J. Gao, Z. Zheng, J. Lv and B. Zhou, *ACS Applied Nano Materials*, 2019, **2**, 3039-3049.

24. D. F. Chai, J. J. Jian, B. N. Li, H. J. Pang, H. Y. Ma, K. Q. Li, B. X. Xiao, X. M. Wang, L. C. Tan, *Dalton Trans.*, 2019,**48**, 13026-13033.